



The Laser-assisted Cold Spray process and deposit characterisation

Matthew Bray^{*}, Andrew Cockburn, William O'Neill

Centre for Industrial Photonics, Institute for Manufacturing, Department of Engineering, University of Cambridge, Cambridge, CB2 1RX, UK

ARTICLE INFO

Article history:

Received 1 October 2008

Accepted in revised form 26 February 2009

Available online 16 March 2009

Keywords:

Laser-assisted Cold Spray

Thermal spray

Titanium

Oxygen

HVOF

ABSTRACT

Laser-assisted Cold Spray (LCS) is a new coating and fabrication process which combines the supersonic powder beam found in Cold Spray (CS) with laser heating of the deposition zone. LCS combines some advantages of CS: solid-state deposition, high build rate and the ability to deposit metals onto a range of substrates, with reduced operating costs which arise from not using a gas heater and replacing helium with nitrogen as the process gas. A system has been developed to impact metallic powder particles onto a substrate which is locally heated using a diode laser. A pyrometer and control system are used to record and maintain impact site temperature. In this study, $50\ \mu\text{m}$ powder particles are measured to be traveling at around $400\ \text{ms}^{-1}$, and heated to temperatures between $450\ ^\circ\text{C}$ and $900\ ^\circ\text{C}$ when they impact the substrates. Build rates of up to $45\ \text{g}\ \text{min}^{-1}$ were achieved for deposits with less than 1% porosity. Oxygen and nitrogen content in the deposits were measured to be less than 0.6 wt.% and 0.03 wt.% respectively.

© 2009 Elsevier B.V. All rights reserved.

1. Introduction

Recent trends in the area of Rapid Prototyping (RP) and Manufacturing (RM) have led to the development of processes which provide end users with metal components that are not simply form and fit prototypes, but allow functional load-bearing testing or actual in-service use [1]. Similar technologies are also used as a means of surface modification and coating of components for increased functionality. Many processes such as laser Laser Engineered Net Shaping (LENS) [2] and Direct Metal Deposition (DMD) [3] are based on laser cladding and sintering, and use a laser to melt and fuse metallic powder into a net or near-net shape on a layer-by-layer basis.

Lasers can also be used with thermal spray processes such as high velocity oxy-fuel (HVOF) [4] or plasma spray [5]. This is typically either a surface preparation step to increase particle–substrate bonding and improve wear resistance [6], or more often as a post-processing step to modify microstructure [4,7].

Drawbacks of high-temperature processes such as laser cladding and traditional thermal spray processes include deposit–substrate dilution, high thermally induced residual stresses, and as-solidified microstructures which lead to component distortion [8] and poor mechanical properties. There is also often a requirement for a high purity inert atmosphere to prevent oxidation during processing [9].

An increasing amount of work is focussing on the development of a non-melting deposition process, known as Cold Spray (CS) and related processes such as Cold Gas Dynamic Manufacturing (CGDM) [10]. In CS, powder is entrained in a supersonic gas jet which accelerates the particles to velocities above their ‘critical velocity’ required for

deposition, often approaching $1000\ \text{ms}^{-1}$ before they impact the substrate. On impact the particles undergo significant plastic deformation which leads to localised heating and flash welding at the interface [11]. This technique can be used to produce thick coatings and components [12]. However there are inherent problems associated with the ‘cold’ mechanism of deposition: high operating costs such as gas consumption and gas heating, inherent compressive residual stresses, and a reduction in bond strength and density when moving from depositing weaker materials to harder, stronger materials such as titanium alloys. While softer materials such as copper or aluminium can be deposited successfully using nitrogen, in order to increase deposition efficiency and deposit higher strength materials it is necessary to increase particle velocity by heating the process gas [13] and, in some cases, replacing nitrogen with helium. Gas heaters currently in use are up to 50 kW and are used to heat substantial amounts (>2000 slpm) of gas to temperatures as high as $800\ ^\circ\text{C}$, which significantly increases both capital and running costs of the process.

Helium is an attractive choice for use as a process gas, as its high sonic velocity leads to increased particle acceleration [14]. In order to sustain sufficient mass flow rates of gas for particle acceleration, and to ensure high powder feedrates do not compromise nozzle performance, the diameter of the throat of the supersonic nozzles used is generally of the order of several millimetres. This, combined with pressures of up to 40 bar which are required to obtain the high speeds needed, means flow rates can easily approach 3000 standard litres per minute (slpm) [12]. Unfortunately this comes at a price; helium is around 30 times more expensive than nitrogen, and for a given operating pressure gas consumption is also higher [10]. This results in total gas cost being 80 times that for nitrogen, as shown in Fig. 1.

^{*} Corresponding author.

E-mail address: mjb214@cam.ac.uk (M. Bray).

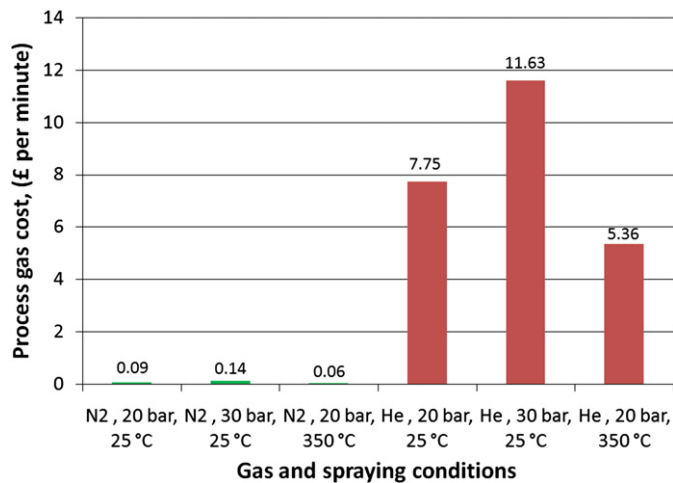


Fig. 1. Comparison of process gas costs [13].

During CS, instantaneous, plastic deformation results in extremely localised heating of the order of one micron [11] around the particle surface. This means that although there is no increase in oxygen and nitrogen levels, hardness of the deposit is increased through cold working or strain-rate hardening [17]. It was suggested by Sakaki and Shimizu [15], modelled by and demonstrated by Dykhuizen and Neiser [16], that an increase in particle temperature can lead to an increase in deposition efficiency and possibly even a reduction in the critical deposition velocity as a result of particle softening [17]. However, increased gas temperatures heighten the risk of nozzle fouling when spraying low melting point metals such as aluminium [18], so a method of heating the metal particles without clogging the deposition nozzle would be essential. Increased deposition temperature may also help to overcome issues of low bond strength in CS coatings, which have been attributed to the extremely short time-scales available for bonding to occur [11].

In Laser-assisted Cold Spray (LCS) impact temperatures are increased though laser heating of the deposition site. This avoids the problems associated with increased process gas temperatures, eliminates the need for gas heating or helium and aims to increase the range of materials which can be deposited. The amount of heat and the rate at which it is applied and removed from the impact zone affects both the rate of deposition and the properties of the material. Increasing particle temperature during traditional thermal spray processing usually increases oxide levels hence hardness [19]. However, during LCS, while there is a temperature increase the material remains non-molten. This means oxide and nitride levels remain comparable to those in CS, but one could expect to see an annealing effect if the deposited particles are cooled at a suitable rate to allow recovery.

LCS will enable the coating, and fabrication of near-net shape components with little or no melting, thus avoiding many of the thermal stressing, distortion, dilution and microstructural problems associated with many laser based technologies. The process was first illustrated in 2006 [20], where a laser was used to heat the deposition site in order to soften the substrate and particles, and allowing aluminium to be deposited using unheated nitrogen at around half the usual gas pressure of CS. The process also shows the capability of allowing deposition to be switched using the laser; when the laser is not on, deposition does not occur as particle velocity is below the CS critical velocity, which may benefit certain applications [21]. Recent work from another research group has been published describing a low-pressure (6 bar) Laser-assisted Cold Spray process for spraying composite metal oxide coatings, which uses similar principles but relies on a powerful laser (6 kW) and gas heating to between 445 °C and 650 °C [22]. Copper and nickel powders were each mixed

with alumina and deposited onto low carbon steel at 2400 mm min⁻¹ – while copper coatings were fully dense, nickel coatings showed porosity at lower temperatures and cracking at higher temperatures.

The aims of this paper are to provide an introduction to the LCS process, detail the particle velocities and temperatures under which deposition occurs, examine the effect of temperature on build rate and coating structure, and compare the coatings produced with those deposited using cold spray and HVOF. Although previous work has used LCS to deposit 316L stainless steel and aluminium, this work focuses on the deposition of titanium tracks and coatings. Titanium was chosen since it is a material which has high value applications in areas such as the biomedical and aerospace industry but which has proven difficult to deposit satisfactorily using CS [26], although recent work has shown coatings produced using a modified HVOF technique [28]. However, the majority of current thermal spray technologies such as plasma spraying involve melting the powder and therefore must be carried out in controlled atmospheres to avoid problems with oxidation [27]. Interstitial oxygen and nitrogen, while increasing the hardness of a coating, generally reduces its ductility and can have a detrimental influence on its cohesion [7]. Coatings with increased hardness and corresponding reduction in ductility means they are more susceptible to cracking which means they may not be suitable for certain applications.

2. Experimental setup and procedures

2.1. LCS equipment

A schematic of the LCS system is shown in Fig. 2. A high pressure (10–30 bar) nitrogen gas supply is split and sent to a converging-diverging (de Laval) nozzle both directly and via a Praxair 1264HP high pressure powder feeder where metal powder particles are entrained. The two streams recombine and pass through the nozzle where they are accelerated to supersonic speeds. The high-velocity, powder-laden gas jet exits the nozzle and is directed towards a substrate. The powder stream impacts a region of the substrate which is simultaneously illuminated by a Laserlines LDL-80 1 kW diode laser of wavelength 980 nm, the deposition zone temperature being monitored with the pyrometer.

The deposition nozzle, laser head and pyrometer are held stationary on the ceiling of a light-tight chamber while the substrate is free to move on a CNC X-Y stage. The chamber is required to be light-tight as the laser is Class IV and the operators control the equipment from within the laboratory. Fig. 3 illustrates the major components within the chamber. Aside from the narrow-size distribution powder used for PIV (particle image velocimetry) measurements, <45 μm

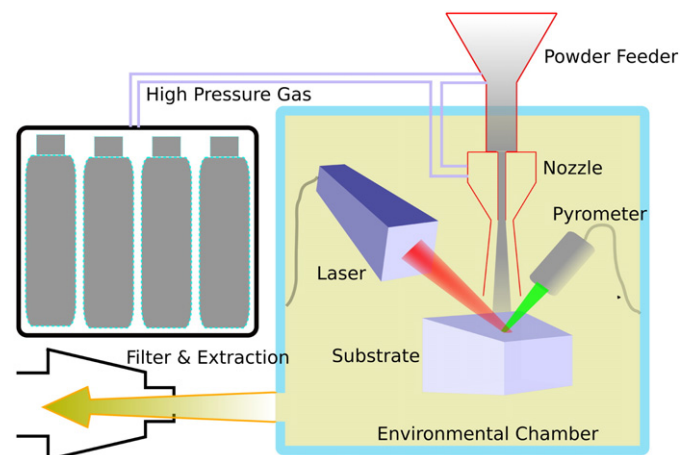


Fig. 2. Layout of the LCS system.

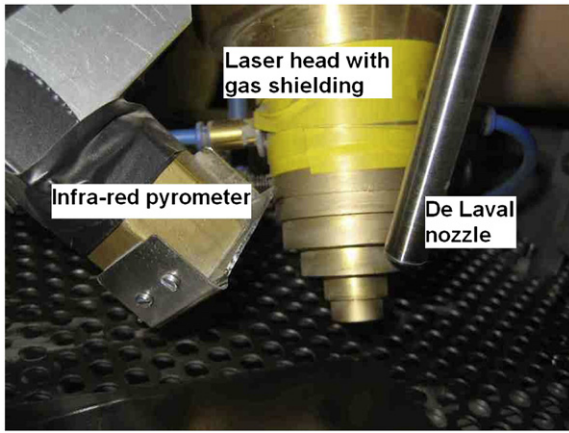


Fig. 3. Layout of LCS system.

spherical titanium powder supplied by Active Metals was deposited onto mild steel substrates. Powder properties can be seen in Table 1.

2.2. Nozzle selection

A range of supersonic deposition nozzles similar to that shown in Fig. 4 had been designed and manufactured as part of the CGDM research programme [10]. It was necessary to determine which of these nozzles performed best under LCS conditions and characterise the relationship between operating pressure and particle velocity. Computational Fluid Dynamics (CFD) was used to assess the performance of each nozzle, whose design parameters are shown in Table 2. Particle velocities predicted for the most appropriate nozzle were then verified experimentally using PIV.

2.3. CFD

The CFD package Fluent™ was used to determine gas and particle velocities produced by each of the available nozzles under the different conditions found in LCS – namely nitrogen instead of helium as the process gas, and at lower pressure and gas temperature than CS. Two dimensional, axi-symmetric methodology was employed to construct the nozzle flow domains using Gambit 2.2.30. The velocity and trajectory of the discrete phase (i.e. the particles) in the two-phase model were computed using a drag force balance written in a Lagrangian reference frame [23]. Particles were injected singly with particle parameters chosen to reflect the powder used in PIV.

2.4. PIV

In order to validate CFD simulations, evaluate nozzle performance and examine in-flight particle behaviour, PIV was used to measure particle displacements and hence derive their velocities [24]. A pair of 30 mJ New Wave Solo PIV II-15 YAG lasers was used to illuminate the flow-field, while a PCO Sencam SVGA Double Exposure camera, capable of image pairs separated by 200 ns was used to take particle images. For this study, the NDLV nozzle and narrow size-distribution

Table 1 Powder types used in this study.

Task	Powder	Size (µm)	Shape	Reason
PIV	316L	22–36	Spherical	Narrow-band size distribution powder gives more consistent reflections for PIV camera
Deposition	Ti	<45µm	Spherical	Easily modeled Cheaper than narrow-band powder Cheaper than narrow-band powder

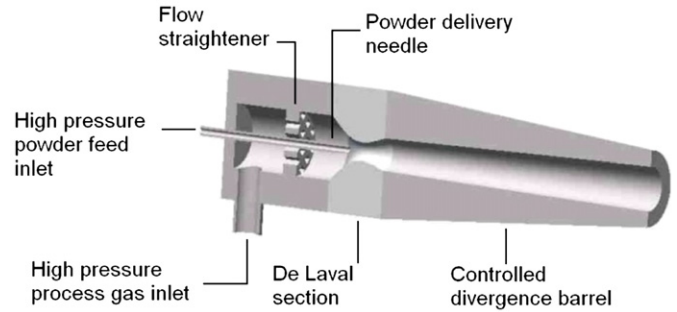


Fig. 4. Supersonic nozzle used in CS and LCS.

316L stainless steel powder were used. The powder was spherical and 22 to 36 µm in diameter.

2.5. Pyrometer

A Kleiber KMGA 740-LO highspeed infrared pyrometer (temperature range 300 to 2500 °C) was used to obtain real-time temperature measurements and control the temperature of the deposition site during the LCS process. The system had a response time of 10 µs and an accuracy of 0.75% of the measured value. Data from the pyrometer was fed through a closed-loop feedback control system which altered laser power as necessary to maintain the desired temperature. The pyrometer was set up to remain coincidental with the powder and laser beam throughout deposition. Emissivity data was supplied by Kleiber [25].

2.6. Sample analysis

Porosity measurements of deposits were found by taking images of polished cross-sections of samples under an optical microscope and using image analysis software to calculate the area fraction of pores within that image.

The level of oxygen and nitrogen in the coatings was determined using the inert gas fusion technique. An ELTRA ONH 2000 Determinator was used which is capable of measuring the oxygen and nitrogen content of metals over the range of 1.10⁻⁵ to 2 wt.%. Measurements were validated through comparison with known standards, feedstock powder and commercially pure CP1 grade titanium sheet.

3. Results

3.1. CFD

CFD was used to model:

- Gas flow through the NDLV, HDLV, HMLN 200, HMLN 150 nozzles.
- Particle velocity through the NDLV, HDLV and HMLN 200 nozzles at 20 bar.

CFD showed a difference of less than 50 ms⁻¹ in gas or particle speeds between the nozzles studied – the NDLV nozzle was selected

Table 2 Supersonic deposition nozzles assessed for performance in the LCS process.

Name	Profile	Length (mm)	Design gas	Design press. (bar)	Design temp. (°C)
NDLV	LDL ^a	180	N ₂	30	400
HDLV	LDL	200	He	20	20
HMLN 150	MLN ^b	150	He	20	20
HMLN 200	MLN	200	He	20	20

^a Linear de Laval.

^b Minimum Length Nozzle (rapid expansion from the throat).

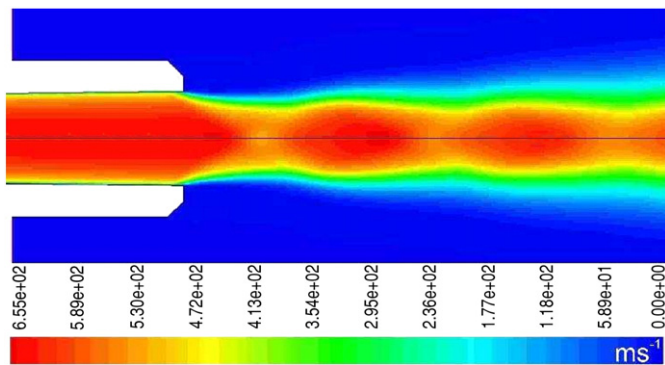


Fig. 5. Gas velocity contours for 30 bar nitrogen through the NDIV nozzle.

for further experiments, as it achieved the highest maximum gas velocity of 655 ms^{-1} , and maximum particle velocity of 442 ms^{-1} for steel and 471 ms^{-1} for titanium particles, as shown in Fig. 6. It should be noted that although beyond the scope of this work, another nozzle could be designed to operate under these specific conditions (i.e. room temperature as opposed to $400 \text{ }^\circ\text{C}$) that would yield better particle velocities – it can be seen from Fig. 5 that the current nozzle is slightly over-expanded which results in a sharp decrease in gas velocity as it leaves the nozzle, but Fig. 6 shows that particle velocity is not dramatically affected.

3.2. PIV data

PIV was used to:

- Measure the velocity distribution across the powder stream to allow comparison with observed track widths.
- Validate CFD predictions through the comparison of centre line velocities with those obtained from CFD.

A PIV measurement, Fig. 7, revealed a well defined powder stream where powder velocity is relatively stable across a central region but drops away very rapidly once the edge of the supersonic jet is reached. Cross sections of velocity showed that particle velocity within 80% of the maximum is maintained over a width of approximately 5 mm up to at least 30 mm from the nozzle exit. Measured velocities were found to be more variable and slightly lower than the CFD model predicted. To form a direct comparison, the average centreline velocities obtained from both PIV and CFD are plotted as a function of operating pressure in Fig. 8.

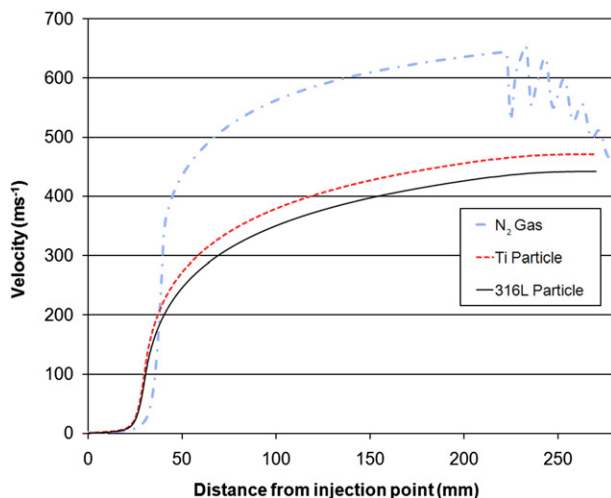


Fig. 6. Gas and particle velocity as a function of position in the LCS nozzle.

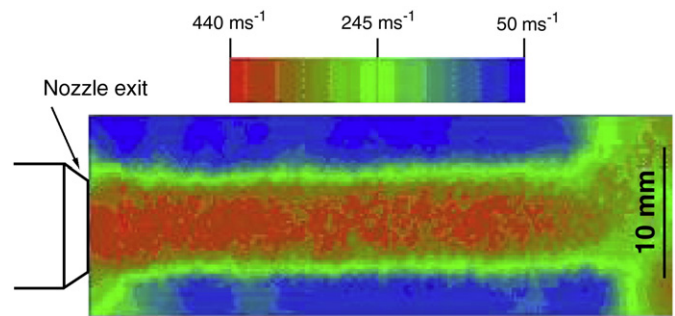


Fig. 7. Velocity distribution at 30 bar outside the nozzle exit measured using PIV.

Good correlation between modelled and measured values can be seen in Fig. 8, with the measured velocities consistently around 20 ms^{-1} ($<5\%$) slower than those predicted by CFD. These results indicate that this CFD model is a suitable tool for assessing performance of the nozzles used in this study, and for determining which is most appropriate for LCS.

3.3. Deposits

Initially, single tracks were sprayed over a range of operating conditions to identify the velocity and temperature ranges required for deposition. In order to quickly identify a process window, the operating pressure was maintained at 30 bar giving particle velocities in the order of 450 ms^{-1} . Deposition site temperature, powder feed rate (PFR) and traverse rate were the parameters examined.

Tracks were deposited under constant spraying conditions of 30 bar unheated nitrogen, a PFR of approximately 40 g min^{-1} and a traverse rate of 500 mm min^{-1} using the control system to vary laser power and maintain a preset temperature.

Using the current equipment, only the central portion of the powder beam was illuminated with the laser – a spot size of diameter 4 mm as opposed to a powder beam diameter of 8 mm. The laser spot size was found by measuring the width of polyimide film burned away when placed at the same standoff distance as the substrate, and the powder beam diameter was found by measuring the diameter of the track that was abraded by the powder on the substrate. It became clear that deposition only occurred within the area of the substrate that was illuminated by the laser. This correlated with pyrometer readings below the lower threshold of the pyrometer's working range ($300 \text{ }^\circ\text{C}$) when the pyrometer was aimed outside of the area illuminated by the laser. The cooling effect of the gas meant that there was little or no

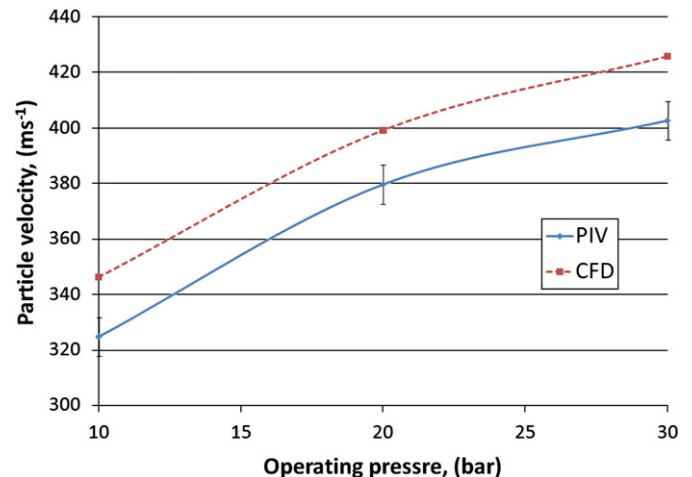


Fig. 8. Comparison of particle velocities measured using PIV with the results of CFD modelling, using N_2 at room temperature as the process gas.

increase in temperature through conduction of heat outside of the area illuminated by the laser, which prevented deposition here. Although powder particles travelling at much the same speed impacted the substrate over a larger area than that being heated, they simply bounced off the substrate, leaving craters similar to those observed in CS when the critical velocity has not been reached [31].

Increased impact site temperature results in an increased deposition rate, as seen in Fig. 9. This may be due to the reduction in strength of particles and substrate with temperature, allowing increased particle deformation and bonding to occur.

Below 450 °C little or no deposition occurred, as shown in Fig. 10, while dense tracks such as the one in Fig. 11, and coatings, as in Fig. 12, were produced from around 550 °C up to 900 °C. This corresponds to a laser power of 650–1000 W using the current system configuration where the laser spot is 4 mm in diameter on the substrate surface. At 1000 W build rates for titanium of up to 25 g or 5.5 cm³ per minute were recorded while at powers less than 650 W, deposit porosity was significantly increased due to insufficient particle consolidation.

SEM examination of the tracks resolved individual particles. Although overall particle deformation is lower than that observed during CS [14], deformation appears to be greater on the top surface of each particle, indicating that cold, hard particles are embedding themselves into a heated, softened substrate during deposition. Three particles have been highlighted to illustrate this in Fig. 13.

Close examination of the coating/substrate boundary reveals an abrupt interface with no third phase material or porosity visible. The level of porosity has been estimated by measuring the area fraction of pores visible in polished sections. Fig. 14 is typical of the deposits produced so far at 500 °C with observed porosity varying from 0.3% to 0.6% over a number of sections.

The deposits produced using LCS have been compared to deposits produced using the CS process using similar powder and equipment. The track shown in Fig. 15 was deposited by traditional CS using helium heated to 300 °C as the process gas, a standoff distance of 50 mm and a nozzle supplied by Cold Gas Technologies. These conditions lead to impact velocities in excess of 800 ms⁻¹ and give rise to a greater degree of particle deformation than that found in LCS. The porosity observed in CS titanium coatings ranges from 2% to 4%.

Also compared were titanium coatings produced using an HVOF system which had been modified to improve temperature control of the carrier gas in order to improve density and reduce oxide contents of coatings, [28]. Here, a trade-off existed between oxide content and porosity, as adding a higher amount of cool nitrogen to the hot carrier gas resulted in oxide content as low as 0.2%, but porosity was increased to 5% (Fig. 16). Adding a lower amount of mixing gas gave porosities as low as 1% but higher oxide contents of over 1%.

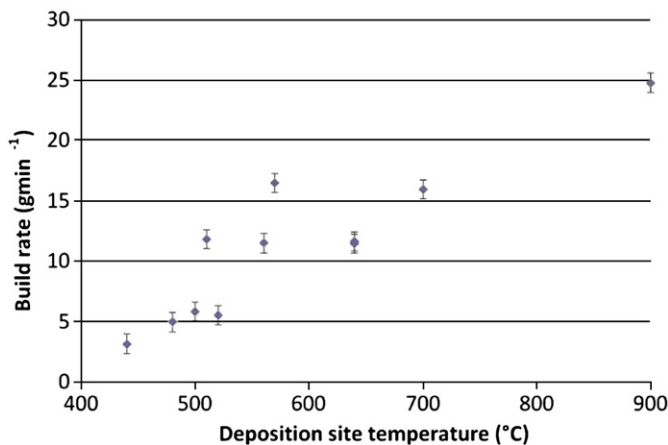


Fig. 9. Build rate versus deposition site temperature for LCS-deposited titanium.

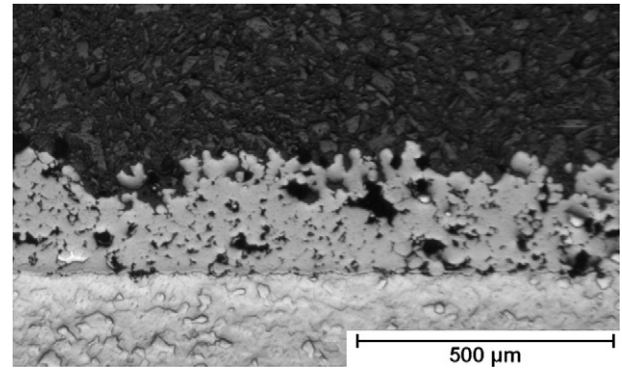


Fig. 10. Optical micrograph showing a cross section through a single titanium LCS track deposited at 450 °C onto a steel substrate.

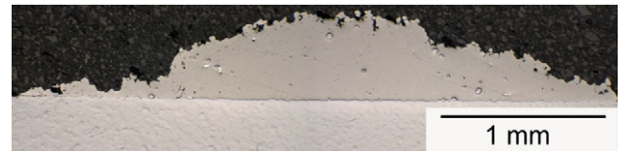


Fig. 11. Titanium track deposited at 550 °C onto a steel substrate.

3.4. Chemical analysis

Oxygen and nitrogen levels were measured in two LCS coatings that had been deposited at 600 °C and 900 °C, and at a fixed traverse rate of 500 mm min⁻¹, the results of these measurements as given in Fig. 17. These were then compared with measurements for cold sprayed titanium, the titanium feedstock powder, and literature values for titanium coatings deposited using modified HVOF.

To determine the level of nitrogen present in the samples with the ELTRA ONH 2000, it was necessary to calibrate the machine and compare results against standard test coupons of known nitrogen concentrations. The test equipment returned values of 45 ppm for a standard coupon containing 0.033 wt.% nitrogen. Both the feedstock powder and the coatings returned values in the range of 30 ppm or below, indicating that true values of nitrogen content for the samples tested lie below the 0.03 wt.% level specified for CP1 grade material. This represents an improvement over the results obtained from analysis of titanium coatings produced from shrouded HVOF which had up to 0.6 wt.% nitrogen for similar sized powder [28].

4. Discussion

CFD and PIV were used to determine which of the available deposition nozzles would accelerate the powder particles to the highest velocities possible under conditions used for LCS. CFD predicted that even though LCS operates using unheated gas, the linear de Laval nozzle that had previously been designed for nitrogen as the working gas at 400 °C would give the best velocities from the nozzles available, and PIV verified these results. It was found that the

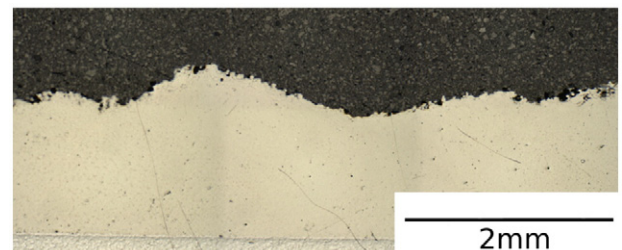


Fig. 12. Titanium coating deposited onto a steel substrate at 550 °C.

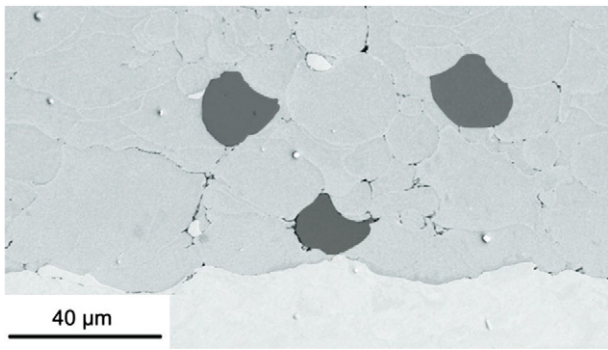


Fig. 13. SEM image of titanium deposited onto steel at 500 °C with deformed particles highlighted.

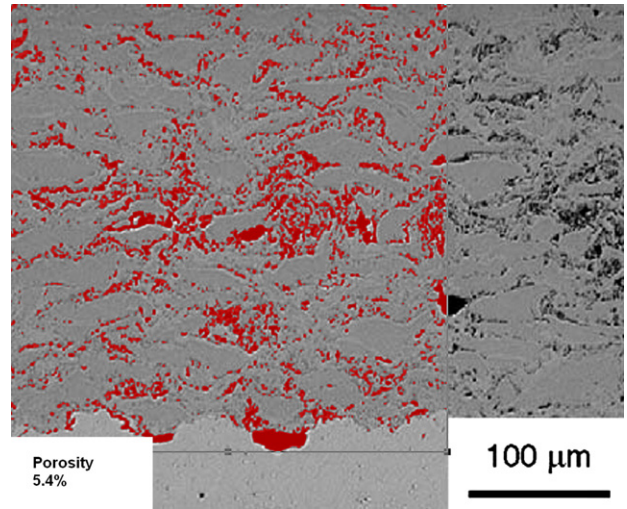


Fig. 16. Micrograph and porosity measurement of HVOF-sprayed titanium [28].

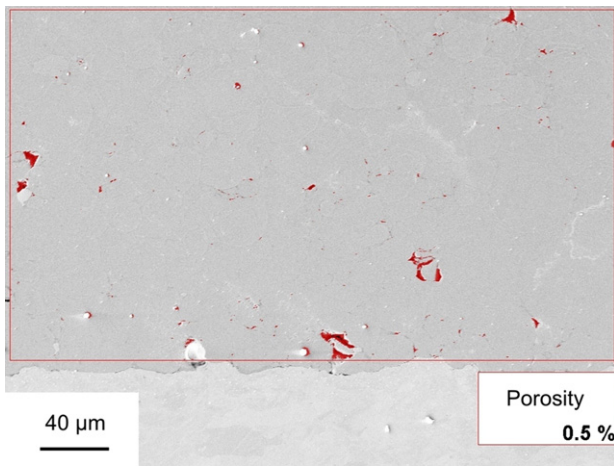


Fig. 14. SEM micrograph of LCS titanium. Pores are highlighted and the area fraction of pores is shown.

titanium particles were accelerated to around 400 ms^{-1} , which is typically less than half the velocities reached in CS and HVOF deposition.

Deposition of titanium using LCS began at around 450 °C. This corresponds to a reduction in 0.2% proof stress of around 65% relative to room temperature [29], which you would expect to reduce critical velocity required for deposition. As deposition site temperature is increased, dense coatings are achieved at 550 °C with build rate increasing up to 900 °C. The increase in build rate with temperature

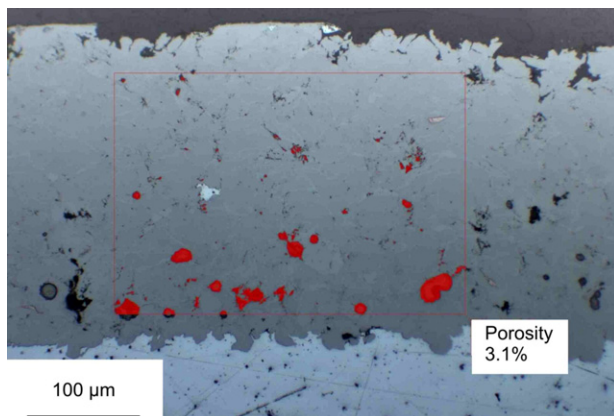


Fig. 15. Micrograph of titanium cold sprayed onto Al. Pores within the measured area are highlighted.

may be a result of a reduction in critical velocity due to increased material softening.

As critical velocity is reduced, the proportion of particles exceeding this velocity will increase leading to an increase in build rate. Above 900 °C, deposited tracks would deform as material was pushed outward by the impinging gas and powder stream, leaving a channel down the centre of each track produced.

The mode of deposition for LCS differs from that seen in CS and HVOF. In CS, when fully dense coatings are formed, a lamellar structure can be seen where particles have elongated horizontal morphologies with random particle indentation, indicating little or no temperature gradient. In HVOF, it can be seen that deposited particles mainly have indentations on their underside, indicating that a relatively hot, soft particle has impacted something relatively cold, and some good micrographs to illustrate this can be seen in [30]. In LCS, deposited particles are seen to have indentations on their top side, indicating that a relatively cold, hard particle has impacted something relatively hot, as seen in Fig. 13. This evidence suggests that in LCS, the temperatures reached at the substrate weaken it and any subsequently deposited material, enough for arriving particles to embed themselves, at which point they also begin heating up. Fully dense deposits, and in particularly those containing titanium, are sought

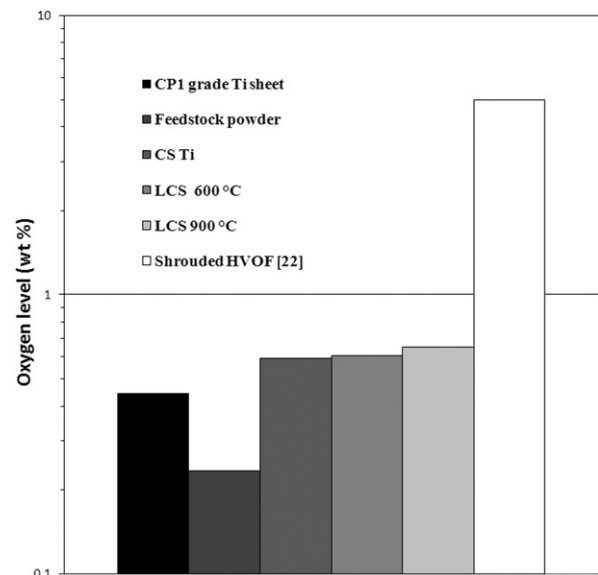


Fig. 17. Oxygen content of LCS titanium coatings, feedstock material and HVOF.

Table 3

Typical build rates and porosity for CS, LCS, Laser Cladding and HVOF.

Process	Material considered	Build rate (g min ⁻¹)	Porosity%
LCS	Ti	<45	<1
CS	Ti	<25	<5
Plasma spraying	Metal oxides	<100	<7
Laser cladding	Ti alloys	<20	<0.1
HVOF	Metal carbides and oxides or alloy matrices	<120	<1

after for corrosion-resistant coatings [7], and the present study has shown that the density of LCS deposits can match those produced using CS, HVOF and laser cladding. Although the LCS coatings show a level of oxygen which exceeds that of the feedstock powder, the values are close to those found for commercially available titanium sheet. Even at the higher deposition temperature, the level of oxygen in the 1000 W (900 °C) coating is similar to that of the 720 W (600 °C) coating. This level of oxygen, 0.6 wt.%, is comparable to that found in cold sprayed titanium coatings and lower than coatings of a similar density produced using the modified HVOF process by Jin et al. Although high temperatures are experienced at the deposition site during LCS, the fact that the particles remain solid during flight and deposition, and experience elevated temperatures for only a limited period of time, may explain why the level of nitrogen and oxygen contamination observed is lower than in traditional thermal spray processes, where elevated temperatures are experienced for the entire duration of the particle flight.

Typical build rate and porosity values for processes mentioned in this paper are given in Table 3. It can be seen that the build rate of LCS compares well when compared to CS, laser cladding and even some HVOF systems. The ability to deposit thick titanium coatings quickly, without melting the substrate, means that the process would be well suited to either repair or strengthening applications on heat sensitive or delicate parts, for example in biomedical implants. The high density of the coatings is an advantage where anticorrosive properties are essential. It should be noted that build rate and deposition efficiency of LCS could be improved with the use of a more powerful laser which could provide the intensity to heat the entire width of the impinging powder beam.

5. Conclusion

LCS has been demonstrated as a viable method for the deposition of metallic coatings, most notably titanium. Oxide-free titanium coatings have been deposited without the use of gas heating at velocities around half of those required in cold spray. For impact velocities of approximately 400 ms⁻¹, dense coatings were produced between 650 and 900 °C, well below the melting point of titanium (1668 °C). The coating structure and impurity content compare well with those observed for cold sprayed and HVOF-sprayed titanium. Although further work is required to achieve greater process control and mechanically characterise the coatings produced, LCS shows the

potential to combine the advantages of a solid-state deposition mechanism similar to that found in CS with lower operating costs and the ability to deposit over selected areas which may make it appropriate for a variety of applications for which CS is unsuited.

Acknowledgment

This research was supported by the Engineering & Physical Sciences Research Council.

References

- [1] T. Wohlers, Wohlers Report, Fort Collins, Colorado, 2007.
- [2] R.R. Unocic, J.N. DuPont, Metall. Mater. Trans. B Proc. Metall. Mater. Proc. Sci. 35 (1) (2004) 143–152.
- [3] J. Mazumder, et al., Opt. Lasers Eng. 34 (4–6) (2000) 397–414.
- [4] T. Schnick, S. Tondou, P. Peyre, L. Pawlowski, S. Steinhäuser, B. Wielage, U. Hofmann, E. Bartnicki, J. Therm. Spray Technol. 8 (2) (1999).
- [5] A. Ohmori, S. Hirano, K. Kamata, J. Therm. Spray Technol. 2 (2) (1993).
- [6] C. Coddet, G. Montavon, S. Ayrault-Costil, O. Freneaux, F. Rigolet, G. Barbezat, F. Folio, A. Diard, P. Wazen, ASM Int. 8 (2) (1999) 235–243.
- [7] L. Pawlowski, The Science and Engineering of Thermal Spray Coatings, Second Edition, 2008.
- [8] R. Vilar, J. Laser Appl. 11 (2) (1999) 64–79.
- [9] K.H. Richter, S. Orban, S. Nowotny, Laser Cladding of the Titanium Alloy Ti6242 to Restore Damage Turbine Blades, International Congress on Applications of Lasers and Electro-Optics, 2004.
- [10] J. Pattison, et al., Int. J. Mach. Tools Manuf. 47 (3–4) (2007) 627–634.
- [11] H. Assadi, et al., Acta Mater. 51 (15) (2003) 4379–4394.
- [12] J. Pattison, J., Ph.D Thesis: Cold Gas Dynamic Manufacturing, in Institute for Manufacturing, Department of Engineering, 2006, University of Cambridge: Cambridge UK.
- [13] V. Champagne, in: V.K. Champagne (Ed.), The Cold Spray Materials Deposition Process, Woodhead Publishing, 2007.
- [14] R. Morgan, et al., Mater. Lett. 58 (7–8) (2004) 1317–1320.
- [15] K. Sakaki, Y. Shimizu, J. Therm. Spray Technol. 10 (3) (2001) 487–496.
- [16] R.C. Dykhuizen, R.A. Neiser, Optimising the Cold Spray Process. In ITSC, ASM International, 2003.
- [17] T. Schmidt, F. Gartner, H. Assadi, H. Kreye, Acta Mater. 54 (2006) 729742.
- [18] T. Stoltenhoff, et al., Optimisation of the Cold Spray Process. In ITSC, ASM International, 2001.
- [19] V.V. Sobolev, J.M. Guilemany, J. Nutting, in: S. Joshi (Ed.), High Velocity Oxy-Fuel Spraying, Maney Publishing, 2004.
- [20] M. Bray, S. Celotto, W. O'Neill, Development of a laser assisted material spraying process, Proceedings of the International Congress on Applications of Laser and Electro-Optics (ICALEO 06), Laser Institute of America, Arizona, USA, 2006, pp. 103–109.
- [21] P.A. Molian, L. Hualun, 130 (1988) 337–352.
- [22] M. Kulmala, P. Vuoristo, Surf. Coat. Technol. 202 (18) (2008) 4503–4508.
- [23] S.A. Morsi, A.J. Alexander, J. Fluid Mech. 55 (2) (1972) 193–208.
- [24] M. Raffel, C. Willert, J. Kompenhans, Particle Image Velocimetry: A Practical Guide, Springer Verlag, Berlin, 1998.
- [25] www.kleiberinfrared.com.
- [26] M. Peters, C. Leyens, Non-Aerospace Applications of Titanium and Titanium Alloys, 2003, pp. 412–416.
- [27] A.E. Segall, J. Met. (1998) 52–54.
- [28] J. Kawakita, S.K. Fukushima Takeshi, Katanoda Hiroshi, H.F. Matsuo Kazuyasu, Surf. Coat. Technol. 201 (2006) 1250–1255.
- [29] E.A. Brandes, G.B. Brook, Smithells Metals Reference Book, Seventh Edition, 1992.
- [30] T. Hanson, C. Hackett, G. Settles, J. Therm. Spray Technol. 11 (1) (2002) 75–85.
- [31] M. Fukumoto, et al., J. Therm. Spray Technol. 16 (5) (2007) 643–650.